Catal Lett (2014) 144:2107–2113
DOI 10.1007/s10562-014-1377-3

Synthesis, Characterization of Ce-doped TiO_2 Nanotubes with High Visible Light Photocatalytic Activity

Panpan Sun · Lei Liu · Shi-Cong Cui · Jin-Gang Liu

Received: 16 July 2014 / Accepted: 22 September 2014 / Published online: 7 October 2014

Abstract Metallic doping effectively extends the light response range of TiO_2 photocatalysts from the ultraviolet (UV) to the visible region. We prepared Ce-doped TiO_2 nanotubes (Ce-TiO_2 NTs) using a sol–gel process followed by a hydrothermal treatment. The Ce-TiO_2 NTs were characterized by X-ray diffraction, transmission electron microscopy, Brunauer–Emmett–Teller surface area, X-ray photoelectron spectroscopy, UV–Vis diffuse reflectance spectroscopy (UV–Vis DRS), and photoluminescence (PL) spectroscopy. Given that the optical absorption was extended to wavelengths of 600 nm, the Ce-TiO_2 NTs demonstrated excellent photocatalytic activity for degrading methylene blue under visible light irradiation. Ce-TiO_2 NTs with various amounts of Ce doping (0.06–0.40 g of cerium nitrate hexahydrate added during preparation) were tested, and the 0.12Ce-TiO_2 NTs showed the highest photocatalytic activity, 7 times higher than that of P25. For their efficient photodegrading of dyes under visible light, these Ce-TiO_2 NTs may be useful for waste water treatment.

Keywords Titanium dioxide · Nanotubes · Cerium · Dopant · Photocatalysis

1 Introduction

Semiconductor photocatalysts have a wide variety of applications, such as sustainable energy generation and environmental pollution treatment. TiO_2 has been one of the most investigated photocatalytic materials, given its efficient photocatalytic activity and high stability [1, 2]. However, for practical photocatalytic applications, pure TiO_2 is limited, because it is only active under ultraviolet (UV) light irradiation due to its large band gap of 3.2 eV for the anatase phase. A variety of methods have been used to enhance the photocatalytic behavior of TiO_2, including non-metal doping [3–6] and metal doping [7–9]. Recently, extensive research has been conducted on the synthesis and characterization of TiO_2 nanotubes owing to their novel properties, such as unique shape, size confinement in the radial direction, and large specific surface area [10–14]. TiO_2 nanotubes combine the properties of layered titanates with the properties and applications of conventional TiO_2 nanoparticles. The unique physicochemical properties of nanostructured titanates, together with their unusual morphology, make these materials very promising for many applications, such as catalysis (photocatalysis, electrocatalysis) [15–21], H_2 storage and separation [22, 23], and lithium batteries [24, 25].

Among the rare earth elements used as photocatalyst dopants, cerium is an efficient electron acceptor that removes photogenerated electrons from electron–hole recombination sites, thereby increasing the quantum yield and enhancing the photocatalytic activity [26–28]. Ce doping is also known to inhibit loss of the catalyst surface area, which can improve catalytic activity, phase stability [29, 30], and preservation of ordered mesoporous structures [31, 32]. Moreover, it can easily form labile oxygen vacancies (OVs) because of the relatively high mobility of bulk oxygen species. Ce-doped TiO_2 nanotubes (Ce-TiO_2 NTs) have previously been prepared through hydrothermal treatment of rutile-phase TiO_2 nanoparticles followed by impregnation of cerium salt, and their use for

P. Sun · L. Liu · S.-C. Cui · J.-G. Liu (✉)
Department of Chemistry, East China University of Science and Technology, 130 Meilong Road, Shanghai 200237, People's Republic of China
e-mail: liujingang@ecust.edu.cn

degradation of glyphosate with a high-pressure mercury lamp as a light source has been demonstrated [33]. Ce-TiO_2 NTs have also been used for flame retardancy of an intumescent flame-retardant polystyrene system [34]. However, there have been no reports on the catalytic performance of Ce-TiO_2 NTs under exclusive visible light conditions. To this end, we prepared Ce-TiO_2 NTs using a sol–gel process followed by hydrothermal treatment, a method different from the previous reported [33–35]. The prepared Ce-TiO_2 NTs were characterized by X-ray diffraction (XRD), transmission electron microscopy (TEM), Brunauer–Emmett–Teller surface area (BET), X-ray photoelectron spectroscopy (XPS), UV–vis diffuse reflectance spectroscopy (UV–Vis DRS), and photoluminescence (PL) spectroscopy. The prepared Ce-TiO_2 NTs demonstrated 7 times more efficient than P25 (commercial TiO_2 nanoparticles) in degrading methylene blue (MB) under visible light conditions. To the best of our knowledge, this study presents the first use of Ce-TiO_2 NTs for degradation of organic materials under exclusive visible light conditions.

2 Experimental Procedures

2.1 Photocatalyst Preparation

Ce-TiO_2 NTs were prepared by a sol–gel process followed by hydrothermal treatment using tetrabutyl titanate (TBOT) as the host precursor and cerium nitrate hexahydrate as the dopant precursor. In a typical synthesis, 10 mL of TBOT was mixed with 10 mL of ethanol to make solution A. Various amounts of cerium nitrate hexahydrate (0.06–0.40 g), depending on the desired doping, together with 0.5 mL of HNO_3, were dissolved in 10 mL of ethanol to make solution B. Then, solution A was slowly added to solution B accompanied by vigorous stirring. After 20 min, 2.5 mL of H_2O was added dropwise to the mixture. The solution first became sol and then gel. The gel stood for 10–12 h and was then dried in an oven at 100 °C followed by a heat treatment at 550 °C for 4 h. The product was Ce-TiO_2. Next, 400 mg Ce-TiO_2 powder was mixed with 50 mL of a 10 M NaOH aqueous solution in a Teflon vessel. This solution was kept at 150 °C for 24 h. Then, the sample was washed with a 0.1 M HCl solution and deionized water, successively. Finally, the particles were dried in an oven at 60 °C. The samples were denoted *x*Ce-TiO_2 NTs, where x was the amount of cerium nitrate hexahydrate added in grams to solution B, as described above.

P25 (TiO_2, 80 % anatase, 20 % rutile, Degussa Co. Ltd.) was used as a control catalyst. Pure TiO_2 NTs were prepared in the absence of Ce-dopant as above described.

2.2 Characterization

Powder XRD was performed on a Rigaku D/MAX-2550 diffractometer with monochromatized Cu Kα radiation ($\lambda = 1.5406$ Å). TEM images were taken with a JEOL JEM-2010. The chemical states of the samples were examined by XPS (Perkin-Elmer PHI 5000C ESCA System) with Al Kα radiation operating at 250 W. UV–Vis DRS of P25 and Ce-TiO_2 NT were recorded in the range from 220 to 800 nm using a Shimadzu UV-2600 spectrophotometer with $BaSO_4$ as a reference. The surface area was determined with a standard BET apparatus (Micrometrics ASAP 2010 N). The PL spectra were measured by a fluorospectrophotometer (Horiba Fluoromax-4) using a Xe lamp as the excitation source at room temperature.

2.3 Measurement of Photocatalytic Properties

The photocatalytic measurements were carried out in an open thermostatic photoreactor. Before light irradiation, a suspension containing 100 mL of 20 mg MB solution and 15 mg of the catalyst was stirred for 30 min in the dark to allow sorption equilibrium. Then, the mixture was irradiated with a 300 W Xenon lamp equipped with a 400 nm cut-off filter. After a given time interval of irradiation, 4 mL aliquots were withdrawn. The residual concentration of MB in the aliquots was analyzed using a UV–vis spectrophotometer.

3 Results and Discussion

3.1 XRD and TEM Analysis

Figure 1 shows the XRD pattern of the Ce-TiO_2 NTs. The spectra of the Ce-TiO_2 NTs displayed peaks arising from titanate NTs [36]. From all the diffraction patterns, it was also clear that the Ce-TiO_2 nanotubes were quite small, as the peaks were very broad. TEM measurements were performed to confirm this morphology. Figure 2 shows typical TEM images of the 0.12Ce-TiO_2 NTs. The needle shapes were nanotubes with outer diameters of approximately 10 nm and lengths of hundreds of nanometers. Figure 2 indicates the nanotubes were hollow and open ended, and their diameters were nearly uniform. TEM examination of the sample indicated the content of NTs was close to 100 %, and the NTs were found been formed in the hydrothermal process.

3.2 BET and XPS Analysis

Figure 3 shows the nitrogen adsorption–desorption isotherm and pore size distribution curve of 0.12Ce-TiO_2 NTs. The

sample exhibited a type IV adsorption isotherm, which is typical of a well-defined mesoporous structure. The pore size distribution was estimated from the desorption branch of the nitrogen isotherm by the Barret–Joyner–Halenda (BJH) method. For the typical 0.12Ce-TiO_2 NTs, the mean pore size and BET surface area were 6.3 nm and 209.6 $m^2\ g^{-1}$, respectively. Compared with P25 ($\sim$50 $m^2\ g^{-1}$), the larger surface area will allow the 0.12Ce-TiO_2 NTs to adsorb more dye molecules and incident light.

The synthesized 0.12Ce-TiO_2 NTs were further characterized by XPS to determine the main elements and chemical states on the TiO_2 surface (Fig. 4). The surface of the 0.12Ce-TiO_2 NTs sample was composed of Ti, O, C, and Ce. The binding energies of Ti $2p_{1/2}$ and Ti $2p_{3/2}$ for the 0.12Ce-TiO_2 NTs sample were at 464.5 and 458.8 eV (Fig. 4b). There was no shift of Ti toward lower binding energy induced by doping with Ce, and Ti existed mainly in the form of Ti^{4+}. Figure 4c illustrates the O 1s spectra for the 0.12Ce-TiO_2 NTs sample. A prominent peak at 530.3 eV is ascribed to Ti–O bonds in TiO_2. Figure 4d shows the Ce 3d XPS of the 0.12Ce-TiO_2 NTs sample. The XPS of Ce 3d was quite complicated owing to the hybridization of Ce 4f with O 2p electrons and the partially-occupied valence of 4f orbitals. According to previous reports, XPS peaks denoted as V_1 (881.8 eV), V_3 (886.3 eV), U_0 (894.9 eV), V_4 (900.4 eV), U_3 (904.1 eV), and U_4 (913.1 eV) can be attributed to Ce^{4+} species, while V_0 (880.5 eV), V_2 (885.3 eV), U_1 (896.9 eV), and U_2 (902.6 eV) can be attributed to Ce^{3+} species [27, 37, 38]. Due to the very weak and complexity of the spectra, it was difficult to get good deconvolution of the spectra. We tentatively to propose that the Ce was probably doped in the structure of TiO_2 NTs, given the apparent similarities of the observed binding energies of Ce^{3+}/Ce^{4+} to those of the Ce-doped TiO_2 [27].

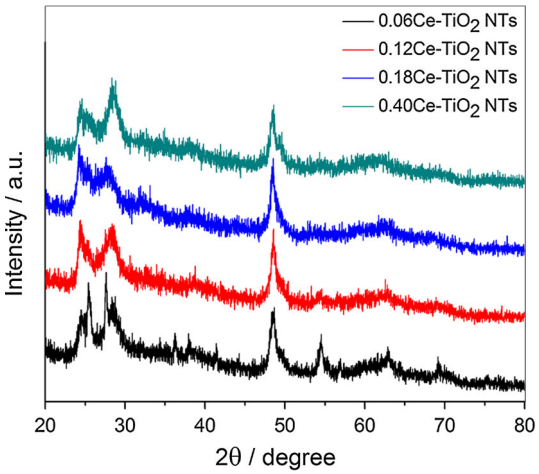

Fig. 1 XRD patterns of the Ce-TiO_2 NTs

3.3 UV–Vis Diffuse Reflectance Spectra Analysis

Figure 5 shows the UV–vis diffuse reflectance spectra for the samples, along with commercial Degussa P25. The samples of Ce-TiO_2 NTs absorb more strongly than the Degussa P25 in the visible light region. The absorbance of Ce-TiO_2 NTs increases with increasing Ce doping. The absorbance of the 0.40Ce-TiO_2 NTs sample in the visible light region was highest among these samples. This indicates that Ce doping can greatly improve the absorption of visible light. Specifically, the 4f electronic configuration of Ce plays a crucial role in generating electron–hole pairs

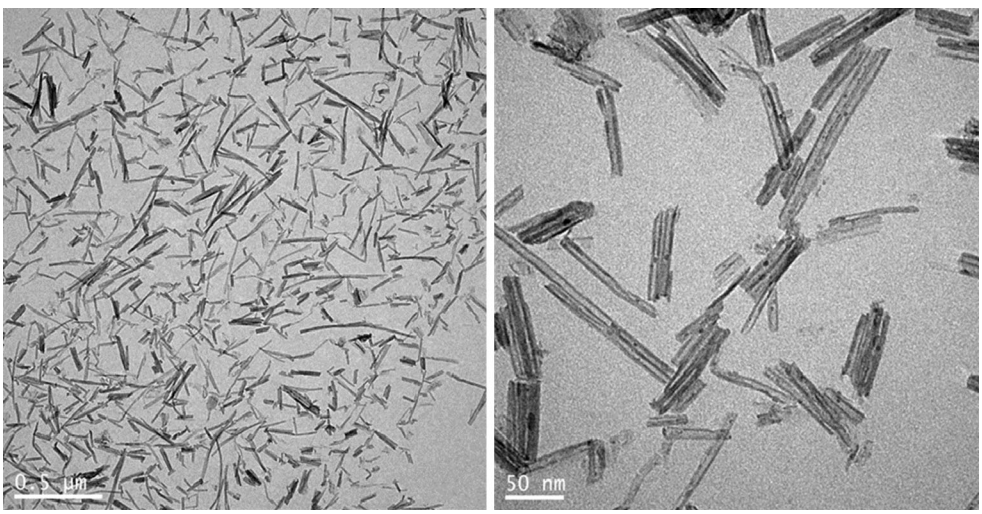

Fig. 2 TEM images of the 0.12Ce-TiO_2 NTs

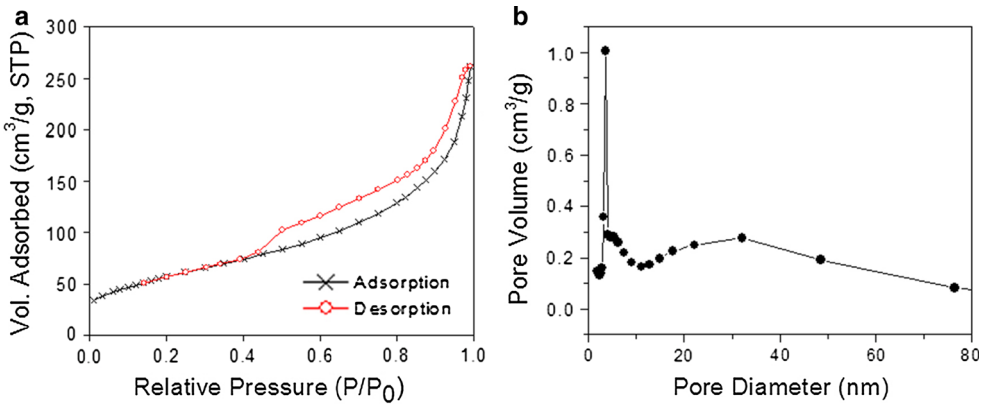

Fig. 3 **a** N_2 adsorption–desorption isotherms and **b** BJH pore size distribution curves for the 0.12Ce-TiO_2 NTs

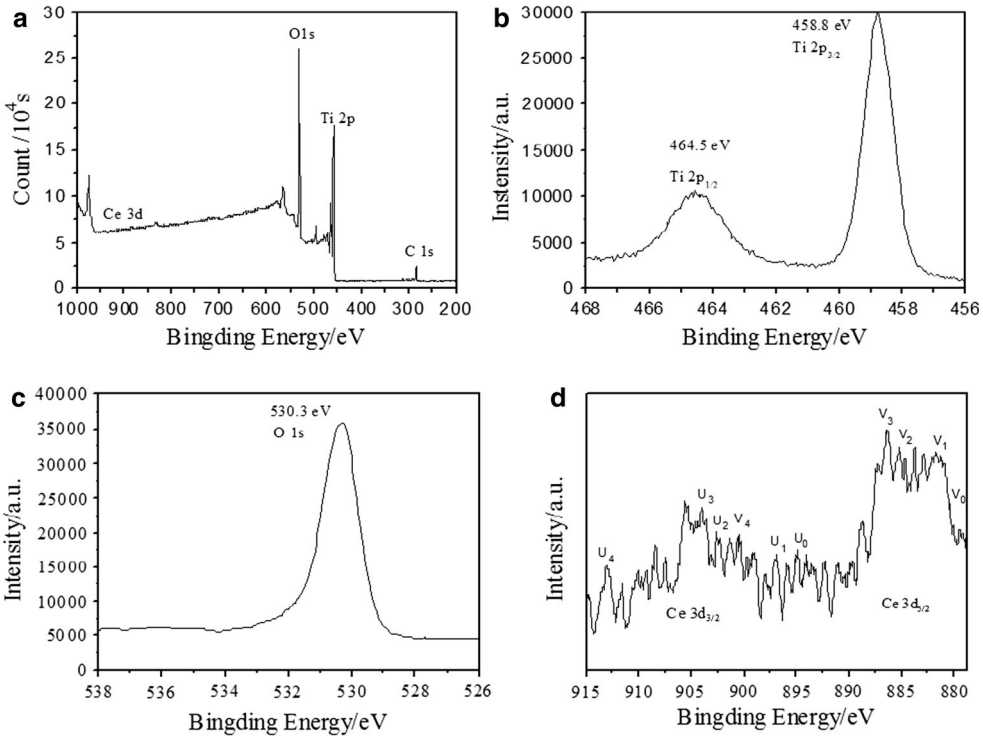

Fig. 4 XPS patterns of the 0.12Ce-TiO_2 NTs: **a** the whole survey; **b** high-resolution spectra of Ti 2p; **c** high-resolution spectra of O 1s; and **d** high-resolution spectra of Ce 3d

with visible light absorption, improving visible light response [39].

3.4 Photocatalytic Measurements

We evaluated the photocatalytic activity of the Ce-TiO_2 NTs by photodegrading MB under visible light ($\lambda > 400$ nm); the result is shown in Fig. 6. Commercial P25 powder and pure TiO_2 NTs were used as control photocatalysts. From Fig. 6, it is clear that Ce-TiO_2 NTs were significantly better for photodegrading MB than P25 as well as pure TiO_2 NTs. Furthermore, the photocatalytic efficiency varied with the amount of Ce in the samples, and the 0.12Ce-TiO_2 NTs exhibited the highest photocatalytic activity. When the Ce amount increases from 0.06 to 0.12 g, there is more of the dominant Ce^{4+} to capture electrons, thus a greater photocatalytic activity. However, if the Ce amount increases from 0.12 to 0.40 g, excess Ce^{4+} may introduce the indirect recombination of electrons and holes, thereby reducing the photocatalytic activity significantly [26]. Under visible light irradiation, 85 % of the initial dyes were decomposed by the 0.12Ce-TiO_2 NTs after 2 h. In contrast, nearly 88 % of the initial dye still remained in the solution with P25 under the same experimental conditions. Several basic factors affect the photocatalytic process, such as light absorption, adsorption of contaminant molecules, and the charge transportation and separation [40, 41]. One reason for the better photocatalytic performance of Ce-TiO_2 NTs is the enhanced adsorption of the MB, which is a prerequisite for good photocatalytic

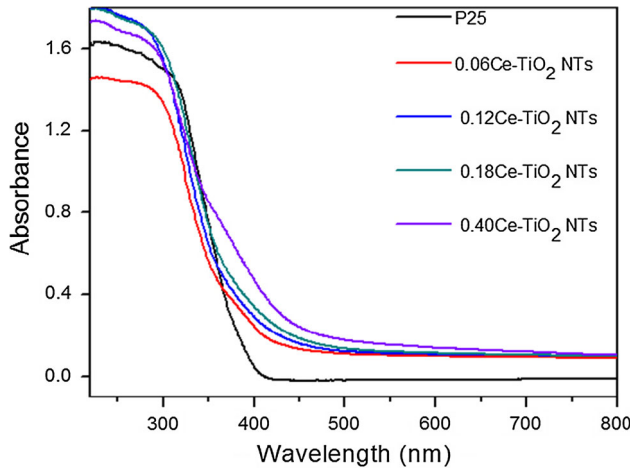

Fig. 5 The UV–vis diffuse reflectance spectrum of P25 and Ce-TiO_2 NTs

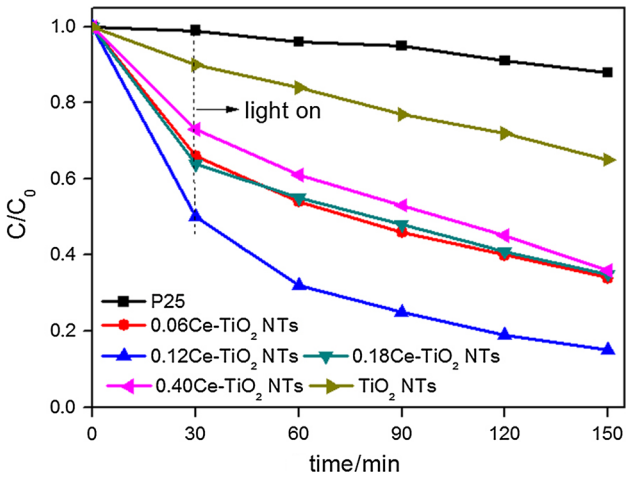

Fig. 6 Photoinduced degradation of MB under visible light in the presence of Ce-TiO_2 NTs, TiO_2 NTs, and P25, respectively

activity [42, 43]. As reactants must collide with Ce-TiO_2 NTs and remain in contact for the photocatalysis to proceed, enhanced adsorption of MB provides a high concentration of reactants close to the surface of the Ce-TiO_2 NTs, thus resulted in the increased photoactivity; while for the non-adsorbed reactants, they just collide with the Ce-TiO_2 NPs by chance, and will pass back into solution and can only react further when they collide with the Ce-TiO_2 NPs again. We observed that after equilibrium in the dark for 30 min, a large amount of dye was adsorbed on the surface of the Ce-TiO_2 NTs, whereas most dye molecules remained in solution with bare P25 as the catalyst. The second reason for the enhanced photocatalytic ability of Ce-TiO_2 NTs is ascribed to the Ce^{4+} dopant. The excited electron can be trapped by Ce^{4+} ions because of its varied valences and special 4f level, as illustrated by the following equations [43, 44]:

$$Ce^{4+} + e^- \rightarrow Ce^{3+}$$

$$Ce^{3+} + O_2 \rightarrow Ce^{4+} + O_2^{\cdot -}$$

$$O_2^{\cdot -} + 2H^+ \rightarrow 2^{\cdot}OH$$

The photoactivity of non-doped pure TiO_2 NTs was much lower than that of the Ce-doped TiO_2 NTs (Fig. 6), indicating the significant role played by the Ce-dopant. This suggested that it was the Ce-dopant rather than the NTs morphology responsible for the enhanced photocatalytic activity. In the meantime, owing to the nanosized effect of the nanotubes, the decrease in electron–hole recombination and fast interfacial charge carrier transfer may have also contributed to the improvement of photocatalytic performance of the 0.12Ce-TiO_2 NTs.

It is worth to note that the photoactivity of the Ce-TiO_2 NTs doesn't necessarily coinside with the samples' absorption trend in the visble region. A little variation of the Ce-dopant amount will influence the photocatalytic performance remarkablely. Only the sample with appropriate amount of Ce-dopant, that is the 0.12Ce-TiO_2 NTs, displayed the highest photoactivity, which was also corroborated by the following PL behavior.

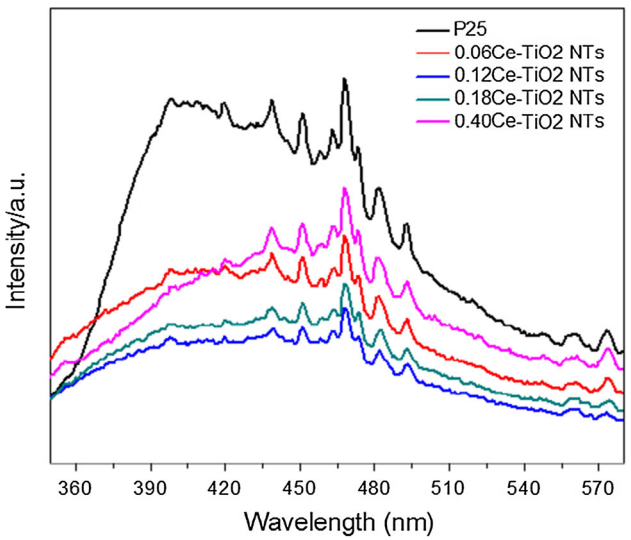

Fig. 7 PL spectra of Ce-TiO_2 NTs samples and P25

3.5 PL Behavior

The PL spectra exhibited the features for excited states and related defects based on the electronic structure and optical characteristics [45–47]. Figure 7 shows the PL spectra of the samples measured with an excitation wavelength of 300 nm at room temperature. PL peaks between 400 and 500 nm were observed for all samples, which indicates

recombination of photogenerated electrons and holes [48, 49]. The 0.12Ce-TiO_2 NTs showed the lowest overall PL compared to the other samples. This indicates the rate of recombination of photogenerated charge carriers was lowest on the surface of the 0.12Ce-TiO_2 NTs. Furthermore, the intensities of the PL spectra increased with increasing Ce beyond 0.12 g, because excess Ce on the surface possibly introduced recombination centers or new trap sites on the surface of the samples [50]. The PL measurement results thus confirmed that the sample with lower intensity of the PL spectrum displays a higher photocatalytic activity.

4 Conclusions

We have demonstrated a new method of preparing Ce-doped TiO_2 NTs, a sol–gel process followed by a hydrothermal treatment. The prepared Ce-TiO_2 NTs exhibited excellent photocatalytic activity for photocatalytic degradation of MB under exclusive visible light conditions. The concentration of the Ce dopant has a great effect on the photocatalytic activity. An appropriate amount of doped Ce is crucial for achieving high photocatalytic activity. The 0.12Ce-TiO_2 NTs sample, with mean pore size of 6.3 nm and high surface area of 209.6 $m^2\ g^{-1}$, showed the highest photocatalytic activity among the tested Ce-doped TiO_2 NTs (0.06Ce–0.40Ce). The 0.12Ce-TiO_2 NTs sample exhibited 7 times higher efficiency than that of P25 in visible light driven degradation of MB, and the prepared Ce-TiO_2 NTs may find potential application in waste water treatment.

Acknowledgments This study was financially supported by NSF of China (#21271072) and the Program for Professor of Special Appointment (Eastern Scholar) at Shanghai Institutions of Higher Learning and was sponsored by the Shanghai Pujiang Program (# 13PJ1401900).

References

1. Fujishima A, Zhang X, Tryk DA (2008) Surf Sci Rep 63:515
2. Hashimoto K, Irie H, Fujishima A (2005) Jpn J Appl Phys 44:8269
3. Lee YF, Chang KH, Hu CC, Lin KM (2010) J Mater Chem 20:5682
4. Asahi R, Morikawa T, Ohwaki T, Aoki K, Taga Y (2001) Science 293:269
5. Li D, Haneda H, Hishata S, Ohashi N, Kolodiazhnyi T, Haneda H (2005) Chem Mater 17:2596
6. Umebayashi T, Yamaki T, Tanaka S, Asai K (2003) Chem Lett 32:330
7. Choi W, Termin A, Hoffmann MR (1994) J Phys Chem 98:13669
8. Subramanian V, Wolf EE, Kamat PV (2003) Langmuir 19:469
9. Zhu JF, Deng ZG, Chen F, Zhang JL, Chen HJ, Anpo M, Huang JZ, Zhang LZ (2006) Appl Catal B 62:329
10. Kasuga T, Hiramatsu M, Hoson A, Sekino T, Niihara K (1998) Langmuir 14:3160
11. Kasuga T, Hiramatsu M, Hoson A, Sekino T, Niihara K (1999) Adv Mater 11:1307
12. Yao BD, Chan YF, Zhang XY, Zhang WF, Yang ZY, Wang N (2003) Appl Phys Lett 82:281
13. Yang JJ, Jin ZS, Wang XD, Li W, Zhang JW, Zhang SL, Guo XY, Zhang ZJ (2003) Dalton Trans 20:3898
14. Bavykin DV, Parmon VN, Lapkin AA, Walsh FC (2004) J Mater Chem 14:3370
15. Lin CH, Chien SH, Chao JH, Sheu CY, Cheng YC, Huang YJ, Tsai CH (2002) Catal Lett 80:153
16. Kleinhammes A, Wagner GW, Kulkarni H, Jia Y, Zhang Q, Qin LC, Wu Y (2005) Chem Phys Lett 411:81
17. Cao J, Sun JZ, Li HY, Hong J, Wang M (2004) J Mater Chem 14:1203
18. Hodos M, Horvath E, Haspel H, Kukovecz A, Konya Z, Kiricsi I (2004) Chem Phys 399:512
19. Xu JC, Lu M, Guo XY, Lia HL (2005) J Mol Catal A 226:123
20. Wang M, Guo DJ, Li HL (2005) J Solid State Chem 178:1996
21. Wang YG, Zhang XG (2004) Electrochim Acta 49:1957
22. Bavykin DV, Lapkin AA, Plucinski PK, Friedrich JM, Walsh FC (2005) J Phys Chem B 109:19422
23. Lim SH, Luo J, Zhong Z, Ji W, Lin J (2005) Inorg Chem 44:4124
24. Zhou YK, Cao L, Zhang FB, He BL, Liz HL (2003) J Electrochem Soc 150:A1246
25. Armstrong AR, Armstrong G, Canales J, Bruce PG (2005) J Power Sources 146:501
26. Xie JM, Jiang DL, Chen M, Li D, Zhu JJ, Lv XM, Yan CH (2010) Colloids Surf A 372:107
27. Li F, Li X, Hou M, Cheah K, Choy W (2005) Appl Catal A 285:181
28. Fang J, Bi XZ, Si DJ, Jiang ZQ, Huang WX (2007) Appl Surf Sci 253:8952
29. Francisco MSP, Mastelaro VR (2002) Chem Mater 14:2514
30. Xiao J, Peng T, Li R, Peng Z, Yan C (2006) J Solid State Chem 179:1161
31. Oveisi H, Jiang X, Nemoto Y, Beitollahi A, Yamauchi Y (2011) Microporous Mesoporous Mater 139:38
32. Yuan S, Chen Y, Shi L, Fang J, Zhang J, Yamashita H (2007) Mater Lett 61:4283
33. Xue WL, Zhang GW, Xu XF, Yang XL, Liu CJ, Xu YH (2011) Chem Eng J 167:397
34. Wu Y, Kan YC, Song L, Hu Y (2012) Polym Adv Technol 23:1612
35. Chen X, Cao S, Weng X, Wang H, Wu Z (2012) Catal Commun 26:178
36. Chen X, Wang H, Gao S, Wu Z (2012) J Collid Interf Sci 377:131
37. Chang LH, Sasirekha N, Chen YW, Wang WJ (2006) Ind Eng Chem Res 45:4927
38. Larachi F, Pierre J, Adnot A, Bernis A (2002) Appl Surf Sci 195:236
39. Liu C, Tang X, Mo C, Qiang Z (2008) J Solid State Chem 181:913
40. Zhang LW, Fu HB, Zhu YF (2008) Adv Funct Mater 18:2180
41. Zhang H, Lv XJ, Li YM, Wang Y, Li JH (2010) ACS Nano 4:380
42. Morales W, Cason M, Aina O, de Tacconi NR, Rajeshwar K (2008) J Am Chem Soc 130:6318
43. Cao XP, Li D, Jing WH, Xing WH, Fan YQ (2012) J Mater Chem 22:15309
44. Nasir M, Xi ZH, Xing MY, Zhang JL, Chen F, Tian BZ, Bagwasi S (2013) J Phys Chem C 117:9520
45. Wang RC, Lin HY (2011) Mater Chem Phys 125:263
46. Zeng HB, Cai WP, Liu PS, Xu XX, Zhou HJ, Klingshirn C, Kalt H (2008) ACS Nano 2:1661

47. Zeng HB, Duan GT, Li Y, Yang SK, Xu XX, Cai WP (2010) Adv Funct Mater 20:561
48. Xu L, Guo Y, Liao Q, Zhang J, Xu D (2005) J Phys Chem B 109:13519
49. Candrinou C, Boukos N, Stogios C, Travlos A (2009) Microelectron J 40:296
50. Nasira M, Bagwasi S, Jiao YC, Chen F, Tian BZ, Zhang JL (2014) Chem Eng J 236:388